Hindawi
Wireless Communications and Mobile Computing
Volume 2022, Article ID 9425490, 15 pages
https://doi.org/10.1155/2022/9425490

Research Article

On the Secrecy Outage Performance of Cooperative NOMA-Assisted Hybrid Satellite-Terrestrial Networks

Bingjing Li,[1] Ding Xu,[1] Bailing Chen,[1] and Ishtiaq Ahmad[2]

[1]*Jiangsu Key Laboratory of Wireless Communications, Nanjing University of Posts and Telecommunications, Nanjing 210003, China*
[2]*Department of Electrical Engineering, University of Lahore, Lahore 54000, Pakistan*

Correspondence should be addressed to Ding Xu; xuding@ieee.org

Received 19 January 2022; Accepted 28 May 2022; Published 10 June 2022

Academic Editor: Tien-Wen Sung

This paper investigates the secrecy outage performance of a downlink cooperative nonorthogonal multiple access- (NOMA-) assisted hybrid satellite-terrestrial network, where a satellite source communicates with two terrestrial users based on NOMA, in the presence of a terrestrial eavesdropper. We assume that there is no direct link between the satellite source and the far terrestrial user, and the near terrestrial user acts as a relay to forward the information to the far terrestrial user. The near user is assumed to support both half-duplex mode and the full-duplex mode for information relaying. We derive the closed-form exact expressions for the secrecy outage probability (SOP) of the near user, as well as the closed-form approximate expressions for the SOP of the far user based on the Gaussian-Chebyshev quadrature. Theoretical results are validated by conducting simulations. The impacts of various system parameters on the performance comparison between the half-duplex mode and full-duplex mode are investigated. Particularly, the full-duplex mode is shown to outperform the half-duplex mode when the received signal-to-noise ratio (SNR) at the near user is low or the residual self-interference is low.

1. Introduction

Integrated/hybrid satellite-terrestrial networks have been proposed to tackle the limitations of standalone satellite networks and terrestrial networks [1]. The main difference between integrated and hybrid satellite-terrestrial networks is that the terrestrial component of an integrated network is controlled by the satellite resource and network management system and uses the same frequency bands as the satellite component, while the terrestrial component of a hybrid network is independent from the satellite component and does not necessarily use the same satellite frequency [2]. In this paper, we do not put restrictions on the relationship between the terrestrial and satellite components in the satellite-terrestrial networks and thus focus on the hybrid satellite-terrestrial networks.

Hybrid satellite-terrestrial networks may face some major challenges, such as the lack of availability of line-of-sight (LoS) link due to obstacles; shadowing effects or weather factors will degrade the communication quality between the terrestrial users and the satellites [3]. In this regard, cooperative technology is an effective method to overcome these challenges by the cooperation between network nodes [4]. Specifically, cooperative technology can be divided into two types: one employs dedicated relays to forward the information to the users with inferior channel condition, and the other one relies on the users with better channel condition to forward the information to the users with inferior channel condition [4]. Most of the existing studies on hybrid satellite-terrestrial networks applied cooperative technology based on dedicated relays to forward the messages from the satellites to the terrestrial users, and such networks are called hybrid satellite-terrestrial relay networks [5, 6].

Meanwhile, nonorthogonal multiple access (NOMA) is a promising technique for improving the spectral efficiency of satellite-terrestrial networks [7, 8]. NOMA uses nonorthogonal transmission technology to superpose information of multiple users in the same time and frequency domain, while the receivers use successive interference cancellation (SIC) technology to decode their information [7, 9]. A key

feature of NOMA technology is that users with better channel conditions can have prior information of other users. By using this prior knowledge, cooperative NOMA (CNOMA) has been utilized to further improve the performance of far users with inferior channel conditions [10–13]. Recently, a large number of studies have applied NOMA on terrestrial users in hybrid satellite-terrestrial relay networks [14, 15]. For example, [14] investigated the outage probability of a NOMA-assisted hybrid satellite-terrestrial relay network and derived the closed-form expression for the outage probability of each NOMA user.

Due to the wide coverage of satellite communications, there are serious security problems for hybrid satellite-terrestrial networks [16–18]. In this respect, physical layer security (PLS) has become a promising technology that complements and significantly improves the security of wireless networks [18] and has been applied in hybrid satellite-terrestrial networks to enhance the security of terrestrial users. It is noted that although applying CNOMA to hybrid satellite-terrestrial networks can improve the performance of far users, almost all existing studies have considered CNOMA with dedicated relays. However, when dedicated relays are not available, cooperation among users needs to be considered. To the best of the authors' knowledge, there is no work on the secrecy outage performance analysis of CNOMA-assisted hybrid satellite-terrestrial networks with user cooperation. Although the secrecy performance of CNOMA-assisted terrestrial networks has been investigated in existing literature such as [11], the current results cannot be directly applied to the hybrid satellite-terrestrial networks, since the channel environments of the hybrid satellite-terrestrial networks are much more complicated than those of the terrestrial networks [19]. This research gap motivates the work in this paper.

The main contributions of this paper are summarized as follows:

(i) We consider a CNOMA-assisted hybrid satellite-terrestrial network with a satellite source, one far terrestrial user, and one near terrestrial user, in the presence of a terrestrial eavesdropper. It is assumed that there is no direct link between the satellite source and the far terrestrial user, and thus, the satellite source sends the information of both users to the near terrestrial user, and then, the near terrestrial user acts as a relay to forward the information to the far terrestrial user under the half-duplex relaying mode or the full-duplex relaying mode. It is also assumed that the eavesdropper wiretaps not only the information broadcast by the satellite source but also the information forwarded by the near terrestrial user

(ii) Under the half-duplex relaying mode and the full-duplex relaying mode of the near user, the closed-form exact expressions for the secrecy outage probability (SOP) of the near terrestrial user are derived, and the closed-form approximate expressions for the SOP of the far terrestrial user are derived based on the Gaussian-Chebyshev quadrature

(iii) Theoretical results are validated by Monte Carlo simulation results. It is shown that the full-duplex relaying mode outperforms the half-duplex relaying mode when the received signal-to-noise ratio (SNR) at the near terrestrial user is low or the residual full-duplex self-interference is low

The rest of this paper is organized as follows. Section 2 introduces the related work. In Section 3, we present the system model. In Sections 4 and 5, the SOPs under the half-duplex mode and the full-duplex mode are investigated, respectively. In Section 6, Monte Carlo simulations are provided to verify our theoretical results, followed by conclusions in Section 7.

2. Related Work

Hybrid satellite-terrestrial relay networks have attracted a lot of research attention. In [6], the outage performance of a hybrid satellite-terrestrial relay network was investigated, and the outage probabilities under two cooperative relaying strategies were theoretically derived. In [20], a multiuser hybrid satellite-terrestrial relay network with opportunistic scheduling was considered, and the approximate as well as the asymptotic expressions for the outage probability were derived. In [21], an uplink satellite-terrestrial relay network with multiple decode-and-forward terrestrial relays was considered, and the closed-form expressions for the outage probability and the throughput were derived under the partial relay selection scheme. In [22], the performance of cognitive-uplink fixed satellite service and terrestrial fixed service was investigated, and an analytical expression for the network capacity was derived. In [23], a satellite and aerial-integrated network with rate-splitting multiple access (RSMA) was considered, and an iterative penalty function-based algorithm was proposed to solve the problem of maximizing the system sum rate. In [24], a secure beamforming scheme for a RSMA-based cognitive satellite-terrestrial network in the presence of multiple eavesdroppers was proposed to maximize the secrecy-energy efficiency.

NOMA or CNOMA has been applied to hybrid satellite-terrestrial networks as well. Specifically, in [15], a NOMA-assisted hybrid satellite-terrestrial relay network with small-cell users and macrocell users was considered, and the closed-form expressions for the outage probabilities were derived. In [25], a satellite multicast network was considered to share the millimeter wave spectrum with a terrestrial network employing NOMA technology, and the system sum rate was maximized by optimizing the beamforming vectors and the power coefficients. In [16], the effect of hardware impairments on the secrecy performance of a NOMA-assisted hybrid satellite-terrestrial relay network was investigated with colluding or noncolluding eavesdroppers, and the closed-form expressions for the SOP under the partial relay selection scheme were derived. In [26], the performance of a NOMA-assisted hybrid satellite-terrestrial relay network was investigated under the partial relay selection scheme and imperfect SIC, and the closed-form expressions for the outage probability and the ergodic capacity were derived.

Besides NOMA and CNOMA, there are other emerging technologies such as reconfigurable intelligent surface (RIS) [27, 28], which have been considered to improve the performance of hybrid satellite-terrestrial networks. For example, in [27], the beamforming was designed to minimize the total transmit power under the user rate constraints for a RIS-aided hybrid satellite-terrestrial relay network.

Physical layer security has been studied in CNOMA networks. In [29], the physical layer security of a two-user CNOMA network, where the strong user acts as a relay for the weak user, in the presence of an eavesdropper, was studied, and the closed-form expressions for SOPs of the two users were derived. The work in [30] extended the work in [29] to a multiantenna scenario. In [31], the secrecy performance of a CNOMA network based on half-duplex and full-duplex amplify-and-forward and decode-and-forward relaying protocols in general κ-μ fading channels was investigated. Physical layer security is also a hot research topic in hybrid satellite-terrestrial networks. In [17], the impacts of the relay selection and user scheduling scheme on the secrecy performance for a hybrid satellite-terrestrial relay network with multiple terrestrial relays were investigated. In [18], a downlink hybrid satellite-terrestrial relay network with multiple terrestrial users with the help from multiple cooperative relays, in the presence of multiple eavesdroppers, was considered; the secrecy performances under amplify-and-forward and decode-and-forward protocols were investigated. In [32], the secrecy performance for a NOMA-assisted hybrid satellite-terrestrial network consisting of a satellite source and multiple terrestrial users with the help from a terrestrial base station was investigated.

To our best knowledge, current works on the secrecy performance of CNOMA-assisted hybrid satellite-terrestrial network networks such as [17, 18, 32] are all based on dedicated cooperative relays. However, when dedicated relays are unavailable, the cooperation among users is desirable. Such consideration motivates the work in this paper to investigate the secrecy performance of CNOMA-assisted hybrid satellite-terrestrial networks with user cooperation.

3. System Model

We consider a CNOMA-based hybrid satellite-terrestrial network consisting of a geosynchronous earth orbit (GEO) satellite source (S) and two terrestrial users (near user D_1 and far user D_2), in the presence of an eavesdropper (E), as shown in Figure 1. The direct transmission link between S and D_2 is assumed to be absent due to shadow fading caused by raining, fog, or other obstacles [18, 20]. We assume that the near user D_1 serves as a decoded and forwarding relay to help in transmitting information to the far user D_2, while E wiretaps the information broadcast by the satellite source S and the information forwarded by the near user D_1 (it is assumed that the eavesdropper equips two receivers: one for decoding the satellite signals and the other one for decoding the terrestrial signals, to eavesdrop the information of both the satellite source and the near user [33]). Let h_{S1}, h_{SE}, h_{12}, and h_{1E} denote the channel coefficients from S to D_1, from S to E, from D_1 to D_2, and from D_1 to E, respectively (the channel state information (CSI) is often assumed to be available for resource scheduling. This can be realized by channel training and estimation [34]. In particular, in the training phase, D_1 broadcasts pilot signal; S and D_2 receive the pilot signal for channel estimation and then feed the CSI back to D_1). Additionally, all the links in the network are considered to be independent and flat fading. Similar to the existing works [16, 35], perfect successive interference cancellation (SIC) is assumed to be available. It is assumed that delay-sensitive services are carried by $D_i, i \in \{1, 2\}$, and there is a minimum rate denoted as $R_i, i \in \{1, 2\}$ required to guarantee the quality of service (QoS) for $D_i, i \in \{1, 2\}$.

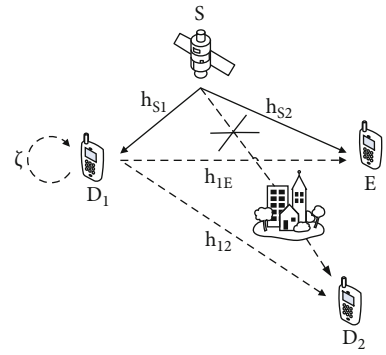

Figure 1: System model.

The satellite links from S to D_1 and from S to E are assumed to follow the shadowed Rician fading model [20, 21, 36], which is the most commonly used channel model in land mobile satellite communication systems [37]. Under the shadowed Rician fading model, the channel coefficient $h_i, i \in \{S1, SE\}$ can be written as

$$h_i = C_i f_i, i \in \{S1, SE\}, \tag{1}$$

where C_i is the scaling parameter including various practical effects such as the free space loss (FSL) and the antenna gain and f_i is the small-scale fading. The C_i can be expressed as [37]

$$C_i = \frac{\lambda}{4\pi} \sqrt{\frac{G_{S,i} G_i}{d_i^2 + {d_0}^2}}, i \in \{S1, SE\}, \tag{2}$$

where λ is the wavelength, d_i is the distance between the terrestrial user and the center of the satellite beam, $d_0 \approx 35786$ km is the height of the GEO satellite, and G_i and $G_{S,i}$ denote the receive antenna gain and the satellite beam gain of the terrestrial user, respectively.

According to [38], $G_i, i \in \{S1, SE\}$ can be expressed as

$$G_i = \begin{cases} \bar{G}_{\max}, & 0^\circ < \beta < 1^\circ, \\ 32 - 25 \log \beta, & 1^\circ < \beta < 48^\circ, \\ -10, & 48^\circ < \beta < 180^\circ, \end{cases} \tag{3}$$

where $\bar{G}_{\max}$ is the maximum antenna gain at the boresight

Table 1: System parameters.

Parameters	Value
Satellite orbit	GEO
Frequency band	$f = 2$ GHz
3 dB angle	$\overline{\theta} = 0.8^{\circ}$
Maximal beam gain	$G_{\max} = 48$ dB
The antenna gain	$G_{k,Sk} = 4$ dB

Table 2: SR fading channel parameters.

Shadowing	m_k	b_k	Ω_k
Frequent heavy shadowing (FHS)	1	0.063	0.0007
Average shadowing (AS)	5	0.251	0.279

and β is the off-boresight angle. Denote by θ the angle between the terrestrial receiver and the satellite beam and by $\overline{\theta}$ the 3 dB angle. The expression for $G_{S,i}, i \in \{S1, SE\}$ is given by [37]

$$G_{S,i} = G_{\max}\left(\frac{J_1(u)}{2u} + 36\frac{J_3(u)}{u^3}\right)^2, \quad i \in \{S1, SE\}, \tag{4}$$

where $G_{\max}$ denotes the maximal beam gain, $u = 2.07123 \sin\theta/\sin\overline{\theta}$, and $J_1(.)$ and $J_3(.)$ represent the first-kind bessel functions of orders 1 and 3, respectively. To attain the best beam gain, we have $\theta \longrightarrow 0$ [39], and thus, $G_{S,i} \approx G_{\max}$ and $C_i = C_i^{\max}, i \in \{S1, SE\}$, where $C_i^{\max} = (\lambda/4\pi)\sqrt{G_{\max}G_i/(d^2 + {d_0}^2)}$.

Under the shadowed Rician fading model, the probability distribution function (PDF) of $|f_i|^2, i \in \{S1, SE\}$ can be described as [16, 21]

$$f_{|f_i|^2}(x) = \alpha_i e^{-\beta_i x}\,{}_1F_1(m_i; 1; \delta_i x), i \in \{S1, SE\}, \tag{5}$$

where $\alpha_i = (1/2b_i)(2b_i m_i/(2b_i m_i + \Omega_i))$, $\beta_i = 1/2b_i$, $\delta_i = \Omega_i/2b_i(2b_i m_i + \Omega_i)$, Ω_i is the average power of the LOS component, $2b_i$ is the average power of the multipath component, m_i is the Nakagami parameter, and ${}_1F_1(a; b; x)$ denotes the confluent hypergeometric function [40].

The terrestrial links from D_1 to D_2 and from D_1 to E are assumed to follow the Rayleigh fading model. Thus, the PDF and the cumulative distribution function (CDF) of $|h_i|^2, i \in \{12, 1E\}$ are given by

$$\begin{aligned} f_{|h_i|^2}(x) &= \frac{1}{\lambda_i}e^{-x/\lambda_i}, \\ F_{|h_i|^2}(x) &= 1 - e^{-x/\lambda_i}, \end{aligned} \tag{6}$$

respectively, where λ_i is the average channel gain.

It is assumed that all the nodes except D_1 are equipped with a single antenna [16, 17, 41]. It is also assumed that D_1 is equipped with one or two antennas. Specifically, D_1 works under the half-duplex mode when only one antenna is available and works under the full-duplex mode when two antennas are available, where one antenna is for transmitting and the other one for receiving. Next, we discuss these two modes.

3.1. Half-Duplex Mode. When D_1 works under the half-duplex mode, the entire transmission time is divided into two phases. In the first time phase, S transmits the superimposed signal (considering hardware impairments is not the focus of this paper. Interested readers may refer to [39, 42]) $\sqrt{P_s\alpha_1}x_1 + \sqrt{P_s\alpha_2}x_2$ to D_1 with $E[|x_i|^2] = 1, i = 1, 2$, where P_s is the transmit power of S and α_i is the power allocation coefficient for x_i. The received signal at D_1 is given by

$$y_1^{HD} = h_{S1}\left(\sqrt{P_s\alpha_1}x_1 + \sqrt{P_s\alpha_2}x_2\right) + n_1, \tag{7}$$

where $n_1 \sim CN(0, \sigma_1^2)$ denotes the additive white Gaussian noise (AWGN) at D_1. It is assumed that D_1 adopts SIC to decode the received message [16, 26]. Specifically, x_2 is decoded first, and then, x_1 is decoded by cancelling the x_2 from the received message (in order to successfully perform SIC, a minimum received power difference is required to distinguish between the desired signal and the interference signal [43]. This means that the difference between the two power allocation coefficients α_1 and α_2 shall be large enough such that SIC can be successfully performed at D_1. It is noted that the performance analysis in this paper does not put restriction on the values of α_1 and α_2. Thus, our analysis is still valid when the values of α_1 and α_2 are set to satisfy the SIC requirement). The signal-to-interference-plus-noise ratio (SINR) at D_1 for decoding x_2 is

$$\gamma_1^{x_2,HD} = \frac{|h_{S1}|^2 P_s\alpha_2}{|h_{S1}|^2 P_s\alpha_1 + \sigma_1^2} = \frac{\gamma_{S1}\alpha_2}{\gamma_{S1}\alpha_1 + 1}, \tag{8}$$

where $\gamma_{S1} = \bar{\gamma}_{S1}|f_{S1}|^2$ and $\bar{\gamma}_{S1} = |C_{S1}^{\max}|^2 P_s/\sigma_1^2$. Then, after applying SIC, the SNR at D_1 to decode its own signal x_1 is given by

$$\gamma^{x_1,HD} = \frac{|h_{S1}|^2 P_s\alpha_1}{\sigma_1^2} = \gamma_{S1}\alpha_1. \tag{9}$$

Meanwhile, since there is a direct link between E and S, the E can also receive the information broadcast by S. Thus, the message received by E is expressed as

$$y_{E,1}^{HD} = h_{SE}\left(\sqrt{P_s\alpha_1}x_1 + \sqrt{P_s\alpha_2}x_2\right) + n_E, \tag{10}$$

where $n_E \sim CN(0, \sigma_E^2)$ denotes the AWGN at E. Here, we consider a worst-case scenario, where E has multiuser detection capability and adopts parallel interference cancellation (PIC) to decode the messages of D_1 and D_2 [16, 44, 45]. Thus, the received SNRs at E to decode the messages x_1

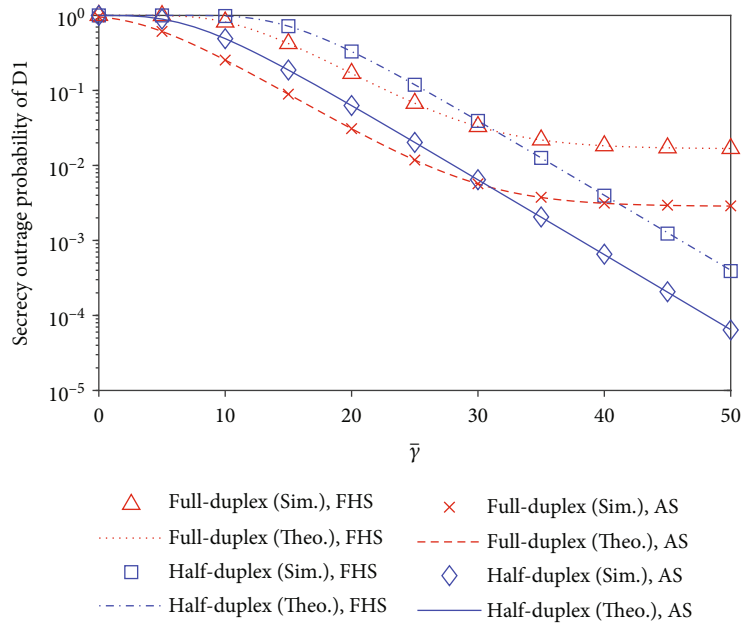

Figure 2: SOP of the near user D_1 versus $\bar{\gamma}$.

and x_2 in the second time phase are

$$\gamma_E^{x_1,HD} = \frac{|h_{SE}|^2 P_s \alpha_1}{\sigma_E^2} = \gamma_{SE}\alpha_1,$$
$$\gamma_{E,1}^{x_2,HD} = \frac{|h_{SE}|^2 P_s \alpha_2}{\sigma_E^2} = \gamma_{SE}\alpha_2, \tag{11}$$

respectively, where $\gamma_{SE} = \bar{\gamma}_{SE}|f_{SE}|^2$ and $\bar{\gamma}_{SE} = |C_{SE}^{\max}|^2 P_s/\sigma_E^2$.

In the second time phase, D_1 forwards the information to D_2, where E can also intercept. The received message at D_2 and E are

$$y_2^{HD} = h_{12}\sqrt{P_R}x_2 + n_2,$$
$$y_{E,2}^{HD} = h_{1E}\sqrt{P_R}x_2 + n_E, \tag{12}$$

respectively, where $n_2 \sim CN(0, \sigma_2^2)$ denotes the AWGN at D_2 and P_R is the transmit power of D_1. Thus, the SNRs at D_2 and E for decoding x_2 in the second time phase can be written as

$$\gamma_2^{x_2,HD} = \frac{|h_{12}|^2 P_R}{\sigma_2^2} = \gamma_{12},$$
$$\gamma_{E,2}^{x_2,HD} = \frac{|h_{1E}|^2 P_R}{\sigma_E^2} = \gamma_{1E}, \tag{13}$$

respectively, where $\gamma_{12} = P_R|h_{12}|^2/\sigma_2^2$ and $\gamma_{1E} = P_R|h_{1E}|^2/\sigma_E^2$. Note that γ_{12} and γ_{1E} follow exponential distributions with mean values $\bar{\gamma}_{12}$ and $\bar{\gamma}_{1E}$, respectively, where $\bar{\gamma}_{12} = P_R/\sigma_2^2$ and $\bar{\gamma}_{1E} = P_R/\sigma_E^2$.

The end-to-end SNR at D_2 for decoding x_2 is the minimum SNR in the two time phases, which can be written as [26]

$$\gamma^{x_2,HD} = \min\left\{\gamma_1^{x_2,HD}, \gamma_2^{x_2,HD}\right\}. \tag{14}$$

As for E to decode x_2, a worst-case scenario is considered, where E adopts the maximal ratio combining (MRC) to combine the x_2 received in the first and the second time phases. Thus, the end-to-end SNR at E for decoding x_2 is

$$\gamma_E^{x_2,HD} = \gamma_{E,1}^{x_2,HD} + \gamma_{E,2}^{x_2,HD}. \tag{15}$$

3.2. Full-Duplex Mode. When D_1 works under the full-duplex mode, during the whole transmission time, S can transmit with the power P_s and the power allocation coefficients α_1 and α_2, while D_1 can forward the information to D_2 with transmit power P_R. The message received by D_1 can be expressed as

$$y_1^{FD} = h_{S1}\left(\sqrt{P_s\alpha_1}x_1 + \sqrt{P_s\alpha_2}x_2\right) + x_{LI} + n_1, \tag{16}$$

where x_{LI} is the residual self-interference signal. We assume that multiple analog and digital self-interference cancellation techniques are adopted to suppress the self-interference. Accordingly, x_{LI} can be modelled as a Gaussian distributed signal which is independent from the transmitted signal due to various affecting factors in the self-interference cancellation procedures [46]. Thus, for the convenience of later analysis, we denote the power of x_{LI} as ζP_R with $0 \le \zeta \le 1$ to identify the relationship between the self-interference signal power and the transmit signal power [47–49].

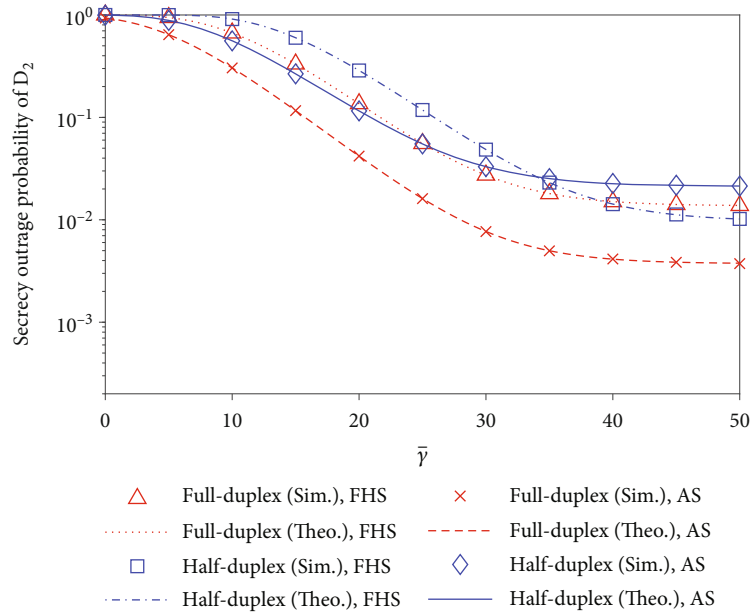

FIGURE 3: SOP of the far user D_2 versus $\bar{\gamma}$.

It is assumed that D_1 decodes x_2 first, and the SINR at D_1 for decoding x_2 is

$$\gamma_1^{x_2,FD} = \frac{|h_{S1}|^2 P_s \alpha_2}{|h_{S1}|^2 P_s \alpha_1 + \zeta P_R + \sigma_1^2} = \frac{\gamma_{S1}\alpha_2}{\gamma_{S1}\alpha_1 + \varpi}, \tag{17}$$

where $\varpi = (\zeta P_R + \sigma_1^2)/\sigma_1^2$. After applying SIC to cancel the x_2 from the received message, the D_1 can proceed to decode x_1, where the SNR for decoding x_1 is

$$\gamma^{x_1,FD} = \frac{|h_{S1}|^2 P_s \alpha_1}{\zeta P_R + \sigma_1^2} = \frac{\gamma_{S1}\alpha_1}{\varpi}. \tag{18}$$

Since D_1 relays x_2 to D_2 with transmit power P_R, the message received by D_2 is

$$y_2^{FD} = h_{12}\sqrt{P_R}x_2 + n_2, \tag{19}$$

and the SNR for decoding x_2 at D_2 is given by

$$\gamma_2^{x_2,FD} = \frac{|h_{12}|^2 P_R}{\sigma_2^2} = \gamma_{12}. \tag{20}$$

Thus, the end-to-end SNR at D_2 for decoding x_2 is the minimum SNR that can be achieved at D_1 and D_2, which is written as

$$\gamma^{x_2,FD} = \min\left\{\gamma_1^{x_2,FD}, \gamma_2^{x_2,FD}\right\}. \tag{21}$$

The message received at E can be written as

$$y_{E,1}^{FD} = h_{SE}\left(\sqrt{P_s\alpha_1}x_1 + \sqrt{P_s\alpha_2}x_2\right) + h_{1E}\sqrt{P_R}x_2 + n_E. \tag{22}$$

It is assumed that E adopts PIC to decode x_1 and x_2, and thus, the SINRs for decoding x_1 and x_2 are given by

$$\gamma_E^{x_1,FD} = \frac{|h_{SE}|^2 P_s \alpha_1}{\sigma_E^2} = \gamma_{SE}\alpha_1, \tag{23}$$

$$\gamma_E^{x_2,FD} = \gamma_{E,1}^{x_2,FD} + \gamma_{E,2}^{x_2,FD}, \tag{24}$$

respectively, where

$$\begin{aligned} \gamma_{E,1}^{x_2,FD} &= \frac{|h_{SE}|^2 P_s \alpha_2}{\sigma_E^2} = \gamma_{SE}\alpha_2, \\ \gamma_{E,2}^{x_2,FD} &= \frac{|h_{1E}|^2 P_R}{\sigma_E^2} = \gamma_{1E}. \end{aligned} \tag{25}$$

4. Secrecy Outage Probability under Half-Duplex Mode

The SOP, defined as the probability that the secrecy rate is below a given threshold [41, 50, 51], is investigated. Under the half-duplex mode, the SOP of $D_i, i \in \{1, 2\}$ is expressed as

$$P_i^{\text{out},HD} = \Pr\left(\left[\frac{1}{2}\log\left(1+\gamma^{x_i,HD}\right) - \frac{1}{2}\log\left(1+\gamma_E^{x_i,HD}\right)\right]^+ < R_i\right), \tag{26}$$

where $[.]^+ = \max\{0,.\}$.

4.1. SOP of the Near User. First, the SOP of D_1 is studied. According to the definition in (26), the SOP of D_1 can be

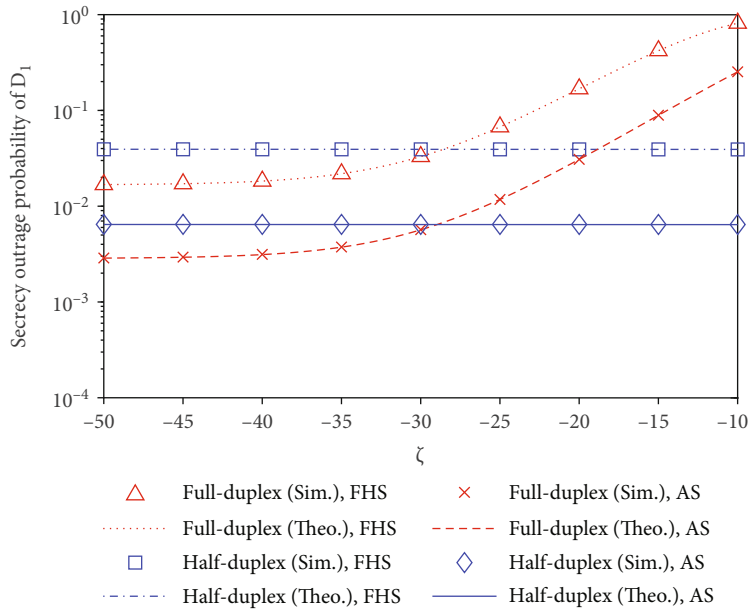

FIGURE 4: SOP of the near user D_1 versus ζ.

expressed as

$$P_1^{\text{out},HD} = \Pr\left(\frac{1}{2}\left[\log\left(1+\gamma^{x_1,HD}\right) - \log\left(1+\gamma_E^{x_1,HD}\right)\right] < \frac{1}{2}\log\left(1+\bar{\gamma}_1^{HD}\right)\right)$$
$$= \Pr\left(\frac{1+\gamma^{x_1,HD}}{1+\gamma_E^{x_1,HD}} < 1+\bar{\gamma}_1^{HD}\right) = \Pr\left(\gamma^{x_1,HD} < \bar{\gamma}_1^{HD} + \gamma_E^{x_1,HD}\left(1+\bar{\gamma}_1^{HD}\right)\right)$$
$$= \int_0^{\infty} \boxtimes f_{\gamma_E^{x_1,HD}}(y) \times F_{\gamma^{x_1,HD}}\left[\bar{\gamma}_1^{HD} + y\left(1+\bar{\gamma}_1^{HD}\right)\right] dy. \tag{27}$$

where $\bar{\gamma}_i^{HD} = 2^{2R_i} - 1$ denotes the SINR for the target secrecy rate denoted as R_i for D_i under the half-duplex mode.

In order to obtain a closed-form expression for $P_1^{\text{out},HD}$, we first deduce the CDF of $\gamma^{x_1,HD}$ and the PDF of $\gamma_E^{x_1,HD}$. Specifically, the CDF of $\gamma^{x_1,HD}$ can be obtained as

$$F_{\gamma^{x_1,HD}}(x) = \Pr(\gamma_{S1}\alpha_1 < x) = F_{\gamma_{S1}}\left(\frac{x}{\alpha_1}\right). \tag{28}$$

From (5), by supposing $\gamma_i = \bar{\gamma}_i |f_i|^2$, $i \in \{S1, SE\}$, the PDF of γ_i can be expressed as

$$f_{\gamma_i}(x) = \frac{\alpha_i}{\bar{\gamma}_i} e^{-\beta_i/\bar{\gamma}_i x}\, {}_1F_1\left(m_i; 1; \frac{\delta_i}{\bar{\gamma}_i} x\right). \tag{29}$$

Under integer m_i, the PDF of γ_i can be rewritten as [16, 21, 32]

$$f_{\gamma_i}(x) = \alpha_i \sum_{k=0}^{m_i-1} \frac{(1-m_i)_k (-\delta_i)^k}{(k!)^2 \bar{\gamma}_i^{k+1}} x^k \exp(-\Delta_i x), \tag{30}$$

where $\Delta_i = (\beta_i - \delta_i)/\bar{\gamma}_i$ and $(\cdot)_k$ is the Pochhammer symbol [40]. Then, the CDF of γ_i, $i \in \{S1, SE\}$ can be calculated as

$$F_{\gamma_i}(x) = 1 - \alpha_i \sum_{k=0}^{m_i-1} \sum_{t=0}^{k} \frac{(1-m_i)_k (-\delta_i)^k}{k! \bar{\gamma}_i^{k+1} t! \Delta_i^{k-t+1}} x^t \exp(-\Delta_i x). \tag{31}$$

By using (31), the CDF of $\gamma^{x_1,HD}$ in (28) can be rewritten as

$$F_{\gamma^{x_1,HD}}(x) = 1 - \alpha_{S1} \sum_{k=0}^{m_{S1}-1} \sum_{t=0}^{k} \frac{(1-m_{S1})_k (-\delta_{S1})^k}{k! \bar{\gamma}_{S1}^{k+1} t! \Delta_{S1}^{k-t+1}} \left(\frac{x}{\alpha_1}\right)^t \exp\left(-\Delta_{S1}\frac{x}{\alpha_1}\right). \tag{32}$$

By following similar procedures, the PDF of $\gamma_E^{x_1,HD}$ can be obtained as

$$f_{\gamma_E^{x_1,HD}}(x) = \frac{1}{\alpha_1} f_{\gamma_{SE}}\left(\frac{x}{\alpha_1}\right)$$
$$= \frac{\alpha_{SE}}{\alpha_1} \sum_{k=0}^{m_{SE}-1} \frac{(1-m_{SE})_k (-\delta_{SE})^k}{(k!)^2 \bar{\gamma}_{SE}^{k+1}} \left(\frac{x}{\alpha_1}\right)^k \exp\left(-\Delta_{SE}\frac{x}{\alpha_1}\right). \tag{33}$$

By substituting (32) and (33) into (27), the $P_1^{\text{out},HD}$ can be obtained as

$$P_1^{\text{out},HD} = \int_0^{\infty} \frac{\alpha_{SE}}{\alpha_1} \sum_{k_1=0}^{m_{SE}-1} \frac{(1-m_{SE})_{k_1} (-\delta_{SE})^{k_1}}{(k_1!)^2 \bar{\gamma}_{SE}^{k_1+1}} \left(\frac{y}{\alpha_1}\right)^{k_1} \exp\left(-\Delta_{SE}\frac{y}{\alpha_1}\right)$$
$$\times \left\{1 - \alpha_{S1} \sum_{k=0}^{m_{S1}-1} \sum_{t=0}^{k} \frac{(1-m_{S1})_k (-\delta_{S1})^k}{k! \bar{\gamma}_{S1}^{k+1} t! \Delta_{S1}^{k-t+1}} \left(\frac{\left[\bar{\gamma}_1^{HD} + y\left(1+\bar{\gamma}_1^{HD}\right)\right]}{\alpha_1}\right)^t \right.$$
$$\left. \times \exp\left(-\Delta_{S1}\frac{\left[\bar{\gamma}_1^{HD} + y\left(1+\bar{\gamma}_1^{HD}\right)\right]}{\alpha_1}\right)\right\} dy. \tag{34}$$

By defining $A_{k,t} = \alpha_{S1}\sum_{k=0}^{m_{S1}-1}\sum_{t=0}^{k}(1-m_{S1})_k(-\delta_{S1})^k/k!\,\bar{\gamma}_{S1}^{k+1}t!\Delta_{S1}^{k-t+1}$ and $B_{k_1} = \alpha_{SE}\sum_{k_1=0}^{m_{SE}-1}(1-m_{SE})_{k_1}(-\delta_{SE})^{k_1}/(k_1!)^2\,\bar{\gamma}_{SE}^{k_1+1}$ and with the help of [40], we can simplify (34) as

$$\begin{aligned}P_1^{\text{out},HD} &= 1-\int_0^{\infty}\frac{A_{k,t}B_{k_1}}{\alpha_1}\left(\frac{y}{\alpha_1}\right)^{k_1}\exp\left(-\frac{\Delta_{SE}y}{\alpha_1}\right)\left(\frac{1}{\alpha_1}\right)^{t}\\&\quad\times\sum_{l=0}^{t}\binom{t}{l}\left(\bar{\gamma}_1^{HD}\right)^{t-l}\left(1+\bar{\gamma}_1^{HD}\right)^{l}y^{l}\\&\quad\times\exp\left(-\Delta_{S1}\frac{\left[\bar{\gamma}_1^{HD}+y\left(1+\bar{\gamma}_1^{HD}\right)\right]}{\alpha_1}\right)dy\\&= 1-\int_0^{\infty}\frac{A_{k,t}B_{k_1}}{\alpha_1^{k_1+t+1}}\sum_{l=0}^{t}\binom{t}{l}\left(\bar{\gamma}_1^{HD}\right)^{t-l}\left(1+\bar{\gamma}_1^{HD}\right)^{l}\\&\quad\times\exp\left(-\frac{\Delta_{S1}\bar{\gamma}_1^{HD}}{\alpha_1}\right)y^{k_1+l}\exp\left(-\frac{\Delta_{SE}+\Delta_{S1}\left(1+\bar{\gamma}_1^{HD}\right)}{\alpha_1}y\right)dy.\end{aligned}\tag{35}$$

Through some simple calculations of (35), the closed-form expression for the SOP of D_1 can be obtained as

$$\begin{aligned}P_1^{\text{out},HD} &= 1-\frac{A_{k,t}B_{k_1}}{\alpha_1^{k_1+t+1}}\sum_{l=0}^{t}\binom{t}{l}\left(\bar{\gamma}_1^{HD}\right)^{t-l}\left(1+\bar{\gamma}_1^{HD}\right)^{l}\exp\left(-\frac{\Delta_{S1}\bar{\gamma}_1^{HD}}{\alpha_1}\right)\\&\quad\times(k_1+l)!\left[\frac{\Delta_{SE}+\Delta_{S1}\left(1+\bar{\gamma}_1^{HD}\right)}{\alpha_1}\right]^{-(k_1+l)-1}.\end{aligned}\tag{36}$$

Remark 1. When $\bar{\gamma}_{S1}$ approaches to infinite, the CDF of γ_{S1} can be approximated as [16, 26]

$$F_{\gamma_{S1}}(x)\approx\frac{\alpha_{S1}}{\bar{\gamma}_{S1}}x+o(x),\tag{37}$$

where $o(x)$ means the infinitesimal of higher order for x. Thus, the $P_1^{\text{out},HD}$ in the high SNR region is approximated as

$$\begin{aligned}P_1^{\text{out},HD,\infty} &= \int_0^{\infty}\frac{B_{k_1}}{\alpha_1}\left(\frac{y}{\alpha_1}\right)^{k_1}\exp\left(-\frac{\Delta_{SE}y}{\alpha_1}\right)\left\{\frac{\alpha_{S1}\left[\bar{\gamma}_1^{HD}+y\left(1+\bar{\gamma}_1^{HD}\right)\right]}{\bar{\gamma}_{S1}\alpha_1}\right\}dy\\&= \frac{B_{k_1}\alpha_{S1}\bar{\gamma}_1^{HD}}{\alpha_1\bar{\gamma}_{S1}\Delta_{SE}^{k_1+1}}(k_1)!+\frac{B_{k_1}\alpha_{S1}\left(1+\bar{\gamma}_1^{HD}\right)}{\bar{\gamma}_{S1}\Delta_{SE}^{k_1+2}}(k_1+1)!.\end{aligned}\tag{38}$$

It is seen from (38) that as $\bar{\gamma}_{S1}\longrightarrow\infty$, the $P_1^{\text{out},HD,\infty}$ approaches to zero. Therefore, the SOP of D_1 does not saturate when the SNR increases.

4.2. SOP of the Far User. Then, we derive the SOP of D_2. The SOP of D_2 can be expressed as

$$\begin{aligned}P_2^{\text{out},HD} &= \Pr\left(\frac{1}{2}\left[\log\left(1+\gamma^{x_2,HD}\right)-\log\left(1+\gamma_E^{x_2,HD}\right)\right]<\frac{1}{2}\log\left(1+\bar{\gamma}_2^{HD}\right)\right)\\&= \int_0^{\infty}f_{\gamma_E^{x_2,HD}}(y)\times F_{\gamma^{x_2,HD}}\left[\bar{\gamma}_2^{HD}+y\left(1+\bar{\gamma}_2^{HD}\right)\right]dy.\end{aligned}\tag{39}$$

To simplify (39), the CDF of $\gamma^{x_2,HD}$ and the PDF of $\gamma_E^{x_2,HD}$ are first derived. The CDF of $\gamma^{x_2,HD}$ is expressed as

$$\begin{aligned}F_{\gamma^{x_2,HD}}(x) &= \Pr\left(\min\left\{\gamma_1^{x_2,HD},\gamma_2^{x_2,HD}\right\}<x\right)\\&= 1-\Pr\left(\min\left\{\gamma_1^{x_2,HD},\gamma_2^{x_2,HD}\right\}\geq x\right)\\&= 1-\underbrace{\Pr\left(\gamma_1^{x_2,HD}\geq x\right)}_{J_1}\underbrace{\Pr\left(\gamma_2^{x_2,HD}\geq x\right)}_{J_2},\end{aligned}\tag{40}$$

where J_1 can be written as

$$J_1=\Pr\left(\frac{\gamma_{S1}\alpha_2}{\gamma_{S1}\alpha_1+1}\geq x\right)=\Pr(\gamma_{S1}(\alpha_2-x\alpha_1)\geq x).\tag{41}$$

Note that when $\alpha_2-x\alpha_1\leq 0$, the inequality $\gamma_{S1}(\alpha_2-x\alpha_1)\geq x$ cannot be satisfied. Thus, we have $J_1=0$ and $F_{\gamma^{x_2,HD}}=1$. Otherwise, when $\alpha_2-x\alpha_1>0$, the J_1 and J_2 can be evaluated as

$$\begin{aligned}J_1 &= \Pr\left(\gamma_{S1}\geq\frac{x}{\alpha_2-x\alpha_1}\right)=1-F_{\gamma_{S1}}\left(\frac{x}{\alpha_2-x\alpha_1}\right)\\&= A_{k,t}\left(\frac{x}{\alpha_2-x\alpha_1}\right)^{t}\exp\left(\frac{-\Delta_{S1}x}{\alpha_2-x\alpha_1}\right),\\J_2 &= \exp\left(-\frac{x}{\bar{\gamma}_{12}}\right),\end{aligned}\tag{42}$$

respectively. Based on the above analysis, the CDF of $\gamma^{x_2,HD}$ is given by

$$F_{\gamma^{x_2,HD}}(x)=\begin{cases}1-A_{k,t}\left(\dfrac{x}{\alpha_2-x\alpha_1}\right)^{t}\exp\left(\dfrac{-\Delta_{S1}x}{\alpha_2-x\alpha_1}-\dfrac{x}{\bar{\gamma}_{12}}\right), & x<\dfrac{\alpha_2}{\alpha_1},\\1, & x\geq\dfrac{\alpha_2}{\alpha_1}.\end{cases}\tag{43}$$

As for the PDF of $\gamma_E^{x_2,HD}$, it can be obtained as [40]

$$\begin{aligned}f_{\gamma_E^{x_2,HD}}(z) &= \int_0^{z}f_{\gamma_{E,1}^{x_2,HD}}(x)f_{\gamma_{E,2}^{x_2,HD}}(z-x)dx\\&= \int_0^{z}\frac{1}{\alpha_2}f_{\gamma_{SE}}\left(\frac{x}{\alpha_2}\right)f_{\gamma_{1E}}(z-x)dx\\&= C_{k_1}\exp\left(-\frac{z}{\bar{\gamma}_{1E}}\right)\left[\frac{k_1!}{\mu^{k_1+1}}-\exp(-\mu z)\sum_{t_1=0}^{k_1}\frac{k_1!}{t_1!}\frac{z^{t_1}}{\mu^{k_1-t_1+1}}\right],\end{aligned}\tag{44}$$

where $C_{k_1}=(\alpha_{SE}/\bar{\gamma}_{1E})\sum_{k_1=0}^{m_{SE}-1}(1-m_{SE})_{k_1}(-\delta_{SE})^{k_1}/(k_1!)^2\bar{\gamma}_{SE}^{-k_1+1}\alpha_2^{k_1+1}$ and $\mu=\Delta_{SE}\bar{\gamma}_{1E}-\alpha_2/\alpha_2\bar{\gamma}_{1E}$.

By substituting (43) and (44) into (39), the $P_2^{\text{out},HD}$ is obtained as given by (45), where $Q^{HD}=\alpha_2-\alpha_1\bar{\gamma}_2^{HD}/\alpha_1(1+\bar{\gamma}_2^{HD})$.

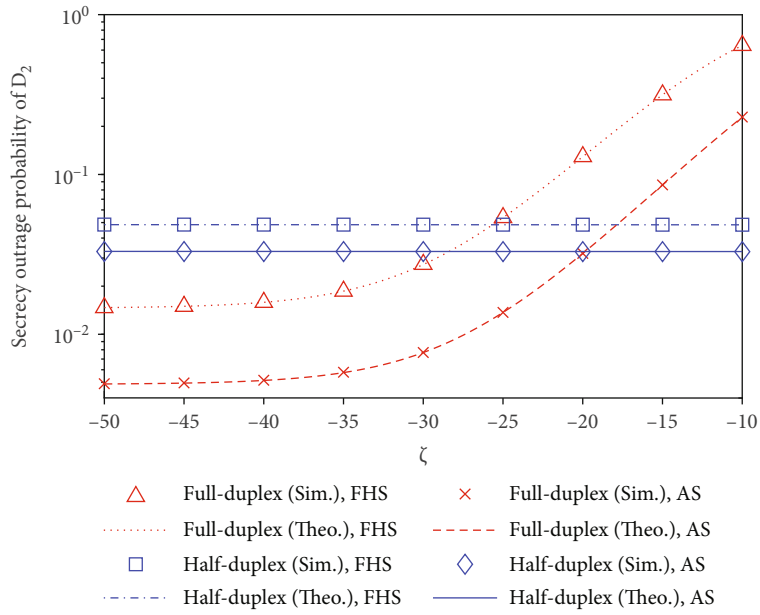

FIGURE 5: SOP of the far user D_2 versus ζ.

$$P_2^{\text{out},HD} = \int_0^{Q^{HD}} f_{\gamma_E^{x_2,HD}}(y)\left\{1 - A_{k,t}\left(\frac{\left[\bar{\gamma}_2^{HD} + y\left(1+\bar{\gamma}_2^{HD}\right)\right]}{\alpha_2 - \left[\bar{\gamma}_2^{HD} + y\left(1+\bar{\gamma}_2^{HD}\right)\right]\alpha_1}\right)^t \exp\left(\frac{-\Delta_{S1}\left[\bar{\gamma}_2^{HD} + y\left(1+\bar{\gamma}_2^{HD}\right)\right]}{\alpha_2 - \left[\bar{\gamma}_2^{HD} + y\left(1+\bar{\gamma}_2^{HD}\right)\right]\alpha_1}\right) \exp\left(-\frac{\left[\bar{\gamma}_2^{HD} + y\left(1+\bar{\gamma}_2^{HD}\right)\right]}{\bar{\gamma}_{12}}\right)\right\} dy + \int_{Q^{HD}}^{\infty} f_{\gamma_E^{x_2,HD}}(y)dy$$
$$= 1 - \underbrace{\int_0^{Q^{HD}} f_{\gamma_E^{x_2,HD}}(y) A_{k,t}\left(\left[\bar{\gamma}_2^{HD} + y\left(1+\bar{\gamma}_2^{HD}\right)\right]/\left(\alpha_2 - \left[\bar{\gamma}_2^{HD} + y\left(1+\bar{\gamma}_2^{HD}\right)\right]\alpha_1\right)\right)^t \exp\left(-\Delta_{S1}\left[\bar{\gamma}_2^{HD} + y\left(1+\bar{\gamma}_2^{HD}\right)\right]/\left(\alpha_2 - \left[\bar{\gamma}_2^{HD} + y\left(1+\bar{\gamma}_2^{HD}\right)\right]\alpha_1\right)\right) \exp\left(-\left[\bar{\gamma}_2^{HD} + y\left(1+\bar{\gamma}_2^{HD}\right)\right]/\bar{\gamma}_{12}\right) dy}_{H_1}. \tag{45}$$

To the best of authors' knowledge, it is hard to derive the exact expression for H_1 in (45). Thus, we adopt the Gaussian-Chebyshev quadrature to approximate H_1 as [52]

$$P_2^{\text{out},HD} \approx 1 - \frac{Q^{HD}}{2}\sum_{i=1}^{K} \omega_i H_1(y_i), \tag{46}$$

where $H_1(y_i)$ is given by (47), K is the number of terms, ω_i is the Gaussian weight, which is given in Table (25.4) of [52], $y_i = (Q^{HD}x_i/2) + (Q^{HD}/2)$, and x_i is the i^{th} zero of Legendre polynomials.

$$H_1(y) = A_{k,t}C_{k_1} \exp\left(-\frac{y}{\bar{\gamma}_{1E}}\right)\left[\frac{k_1!}{\mu^{k_1+1}} - \exp(-\mu y)\sum_{t_1=0}^{k_1}\frac{k_1!}{t_1!}\frac{y^{t_1}}{\mu^{k_1-t_1+1}}\right] \times \left(\frac{\left[\bar{\gamma}_2^{HD} + y\left(1+\bar{\gamma}_2^{HD}\right)\right]}{\alpha_2 - \left[\bar{\gamma}_2^{HD} + y\left(1+\bar{\gamma}_2^{HD}\right)\right]\alpha_1}\right)^t \exp\left(\frac{-\Delta_{S1}\left[\bar{\gamma}_2^{HD} + y\left(1+\bar{\gamma}_2^{HD}\right)\right]}{\alpha_2 - \left[\bar{\gamma}_2^{HD} + y\left(1+\bar{\gamma}_2^{HD}\right)\right]\alpha_1}\right) \exp\left(-\frac{\left[\bar{\gamma}_2^{HD} + y\left(1+\bar{\gamma}_2^{HD}\right)\right]}{\bar{\gamma}_{12}}\right). \tag{47}$$

Remark 2. In the high SNR region, i.e., $\bar{\gamma}_{S1} \longrightarrow \infty$ and $\bar{\gamma}_{12} \longrightarrow \infty$, we have $\gamma_1^{x_2,HD} \approx \alpha_2/\alpha_1$ and $\gamma^{x_2,HD} = \alpha_2/\alpha_1$. Thus, $P_2^{\text{out},HD}$ can be approximated as

$$\begin{aligned} P_2^{\text{out},HD,\infty} &= \Pr\left(\frac{\alpha_2}{\alpha_1} < \bar{\gamma}_2^{HD} + \gamma_E^{x_2,HD}\left(1+\bar{\gamma}_2^{HD}\right)\right) \\ &= \Pr\left(\frac{\alpha_2 - \alpha_1\bar{\gamma}_2^{HD}}{\alpha_1\left(1+\bar{\gamma}_2^{HD}\right)} < \gamma_E^{x_2,HD}\right) \\ &= \underbrace{\int_{Q^{HD}}^{\infty} C_{k_1} \exp\left(-y/\bar{\gamma}_{1E}\right)\left(k_1!/\mu^{k_1+1}\right)dy}_{J_3} - \underbrace{\int_{Q^{HD}}^{\infty} C_{k_1} \exp\left(-y/\bar{\gamma}_{1E}\right)\exp\left(-\mu y\right)\sum_{t_1=0}^{k_1}\left(k_1!/t_1!\right)\left(y^{t_1}/\mu^{k_1-t_1+1}\right)dy}_{J_4}, \end{aligned} \tag{48}$$

where J_3 and J_4 can be obtained as

$$\begin{aligned} J_3 &= C_{k_1}\bar{\gamma}_{1E}\frac{k_1!}{\mu^{k_1+1}}\exp\left(-\frac{Q^{HD}}{\bar{\gamma}_{1E}}\right), \\ J_4 &= C_{k_1}\sum_{t_1=0}^{k_1}\frac{1}{\mu^{k_1-t_1+1}}\sum_{l=0}^{t_1}\frac{k_1!}{l!}\frac{\left(Q^{HD}\right)^l}{\left(1+\mu\bar{\gamma}_{1E}/\bar{\gamma}_{1E}\right)^{t_1-l+1}}, \end{aligned} \tag{49}$$

respectively. It can be shown that, unlike D_1, the SOP of D_2 saturates in the high SNR region.

Remark 3. Note that when $\alpha_1 \geq 1/(1+\bar{\gamma}_2^{HD})$, we have $Q^{HD} \leq 0$, and thus, the SOP of user D_2 is 1. This means that the power allocation coefficient for D_1 shall be smaller than $1/(1+\bar{\gamma}_2^{HD})$; otherwise, D_2 will be always in secrecy outage.

5. Secrecy Outage Probability under Full-Duplex Mode

This section derives the SOPs of all the users under the full-duplex mode. The SOP for D_i, $i \in \{1,2\}$ can be expressed as

$$P_i^{\text{out},FD} = \Pr\left(\left[\log\left(1+\gamma^{x_i,FD}\right) - \log\left(1+\gamma_E^{x_i,FD}\right)\right]^+ < R_i\right). \tag{50}$$

5.1. SOP of the Near User. First, the SOP of the near user D_1 under the full-duplex mode is studied. The SOP of D_1 can be rewritten as

$$P_1^{\text{out},FD} = \int_0^{\infty} f_{\gamma_E^{x_1,FD}}(y) \times F_{\gamma^{x_1,FD}}\left[\bar{\gamma}_1^{FD} + y\left(1+\bar{\gamma}_1^{FD}\right)\right]dy. \tag{51}$$

where $\bar{\gamma}_1^{FD} = 2^{R_i} - 1$ is the SNR for the target secrecy rate R_i for D_i under the full-duplex mode.

From (18), (23), (30), and (31), the CDF of $\gamma^{x_1,FD}$ and the PDF of $\gamma_E^{x_1,FD}$ can be derived as

$$F_{\gamma^{x_1,FD}}(x) = 1 - A_{k,t}\left(\frac{\varpi x}{\alpha_1}\right)^t \exp\left(-\Delta_{S1}\frac{\varpi x}{\alpha_1}\right), \tag{52}$$

$$f_{\gamma_E^{x_1,FD}}(x) = \frac{B_{k_1}}{\alpha_1}\left(\frac{x}{\alpha_1}\right)^{k_1}\exp\left(-\Delta_{SE}\frac{x}{\alpha_1}\right), \tag{53}$$

respectively. By inserting (52) and (53) into (51), we get

$$\begin{aligned} P_1^{\text{out},FD} &= \int_0^{\infty}\frac{B_{k_1}}{\alpha_1}\left(\frac{y}{\alpha_1}\right)^{k_1}\exp\left(-\Delta_{SE}\frac{y}{\alpha_1}\right) \\ &\quad\times\left\{1 - A_{k,t}\left(\frac{\varpi\left[\bar{\gamma}_1^{FD} + y\left(1+\bar{\gamma}_1^{FD}\right)\right]}{\alpha_1}\right)^t\right. \\ &\quad\left.\times\exp\left(-\Delta_{S1}\frac{\varpi\left[\bar{\gamma}_1^{FD} + y\left(1+\bar{\gamma}_1^{FD}\right)\right]}{\alpha_1}\right)\right\} \\ &= 1 - \frac{A_{k,t}B_{k_1}\varpi^t}{\alpha_1^{k_1+t+1}}\sum_{l=0}^{t}\binom{t}{l}\left(\bar{\gamma}_1^{FD}\right)^{t-l}\left(1+\bar{\gamma}_1^{FD}\right)^l(k_1+l)! \\ &\quad\times\exp\left(-\frac{\Delta_{S1}\varpi\bar{\gamma}_1^{FD}}{\alpha_1}\right)\left[\frac{\Delta_{SE}+\Delta_{S1}\varpi\left(1+\bar{\gamma}_1^{FD}\right)}{\alpha_1}\right]^{-(k_1+l)-1}. \end{aligned} \tag{54}$$

Remark 4. In the high SNR region, i.e., $\bar{\gamma}_{S1} \longrightarrow \infty$ and $\bar{\gamma}_{12} \longrightarrow \infty$, the SOP of D_1 can be approximated as

$$P_1^{\text{out},FD,\infty} = \frac{B_{k_1}\zeta\alpha_{S1}\bar{\gamma}_1^{FD}}{\alpha_1\Delta_{SE}^{k_1+1}}(k_1)! + \frac{B_{k_1}\zeta\alpha_{S1}\left(1+\bar{\gamma}_1^{FD}\right)}{\Delta_{SE}^{k_1+2}}(k_1+1)!. \tag{55}$$

It can be shown that the SOP of user D_1 saturates in the high SNR region. This is because the residual self-interference restricts the achievable secrecy rate of D_1 under the full-duplex mode.

5.2. SOP of the Far User. Then, we investigate the SOP of D_2, which can be expressed as

$$P_2^{\text{out},FD} = \int_0^{\infty} f_{\gamma_E^{x_2,FD}}(y) \times F_{\gamma^{x_2,FD}}\left[\bar{\gamma}_2^{FD} + y\left(1+\bar{\gamma}_2^{FD}\right)\right]dy. \tag{56}$$

Similar to (43), the CDF of $\gamma^{x_2,FD}$ can be derived as

$$F_{\gamma^{x_2,FD}}(x) = \begin{cases} 1 - A_{k,t}\left(\dfrac{\varpi x}{\alpha_2 - x\alpha_1}\right)^t \exp\left(\dfrac{-\Delta_{S1}\varpi x}{\alpha_2 - x\alpha_1} - \dfrac{x}{\bar{\gamma}_{12}}\right), & x < \dfrac{\alpha_2}{\alpha_1}, \\ 1, & x \geq \dfrac{\alpha_2}{\alpha_1}. \end{cases} \tag{57}$$

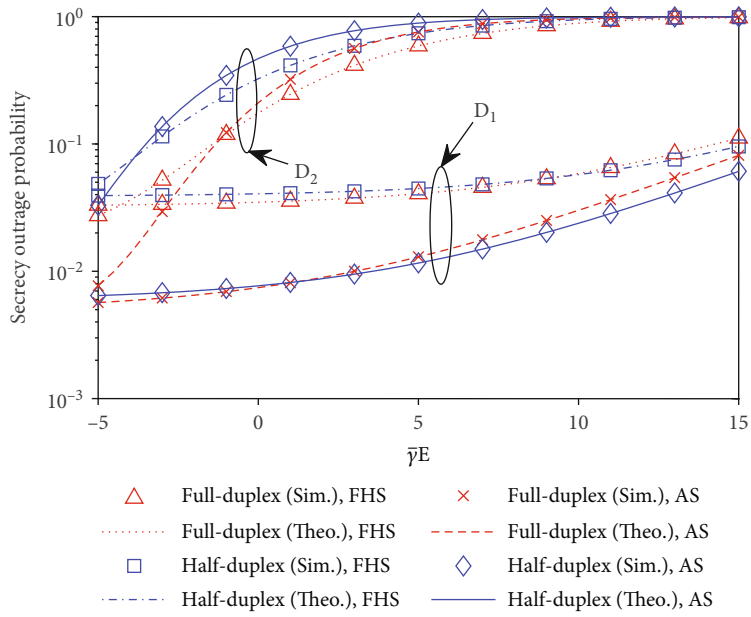

Figure 6: SOP versus $\bar{\gamma}_E$.

The PDF of $\gamma_E^{x_2,FD}$ is derived as

$$f_{\gamma_E^{x_2,FD}}(z) = C_{k_1} \exp\left(-\frac{z}{\bar{\gamma}_{1E}}\right)\left[\frac{k_1!}{\mu^{k_1+1}} - \exp(-\mu z)\sum_{t_1=0}^{k_1}\frac{k_1!}{t_1!}\frac{z^{t_1}}{\mu^{k_1-t_1+1}}\right]. \tag{58}$$

By substituting (57) and (58) into (56), the $P_2^{\text{out},FD}$ can be derived as given by (59), where $Q^{FD} = (\alpha_2 - \alpha_1\bar{\gamma}_2^{FD})/\alpha_1(1+\bar{\gamma}_2^{FD})$.

$$P_2^{\text{out},FD} = 1 - \underbrace{\int_0^{Q^{FD}} f_{\gamma_E^{x_2,FD}}(y) A_{k,t}\left(\varpi\left[\bar{\gamma}_2^{FD} + y\left(1+\bar{\gamma}_2^{FD}\right)\right]/\left(\alpha_2 - \left[\bar{\gamma}_2^{FD} + y\left(1+\bar{\gamma}_2^{FD}\right)\right]\alpha_1\right)\right)^t \exp\left(-\Delta_{S1}\varpi\left[\bar{\gamma}_2^{FD} + y\left(1+\bar{\gamma}_2^{FD}\right)\right]/\left(\alpha_2 - \left[\bar{\gamma}_2^{FD} + y\left(1+\bar{\gamma}_2^{FD}\right)\right]\alpha_1\right)\right) \exp\left(-\left[\bar{\gamma}_2^{FD} + y\left(1+\bar{\gamma}_2^{FD}\right)\right]/\bar{\gamma}_{12}\right) dy}_{H_2}. \tag{59}$$

Since it is hard to derive an exact closed-form expression for $P_2^{\text{out},FD}$, similar to the half-duplex mode, with the help of Gaussian-Chebyshev quadrature, $P_2^{\text{out},FD}$ in (59) can be approximated as [52]

$$P_2^{\text{out},FD} \approx 1 - \frac{Q^{FD}}{2}\sum_{i=1}^{K}\omega_i H_2(y_i), \tag{60}$$

where $H_2(y_i)$ is given by (61) and $y_i = Q^{FD}x_i/2 + Q^{FD}/2$.

$$\begin{aligned} H_2(y) = {} & A_{k,t}C_{k_1}\exp\left(-\frac{y}{\bar{\gamma}_{1E}}\right)\left[\frac{k_1!}{\mu^{k_1+1}} - \exp(-\mu y)\sum_{t_1=0}^{k_1}\frac{k_1!}{t_1!}\frac{y^{t_1}}{\mu^{k_1-t_1+1}}\right] \\ & \times\left(\frac{\varpi\left[\bar{\gamma}_2^{FD} + y\left(1+\bar{\gamma}_2^{FD}\right)\right]}{\alpha_2 - \left[\bar{\gamma}_2^{FD} + y\left(1+\bar{\gamma}_2^{FD}\right)\right]\alpha_1}\right)^t \\ & \exp\left(\frac{-\Delta_{S1}\varpi\left[\bar{\gamma}_2^{FD} + y\left(1+\bar{\gamma}_2^{FD}\right)\right]}{\alpha_2 - \left[\bar{\gamma}_2^{FD} + y\left(1+\bar{\gamma}_2^{FD}\right)\right]\alpha_1}\right) \\ & \exp\left(-\frac{\left[\bar{\gamma}_2^{FD} + y\left(1+\bar{\gamma}_2^{FD}\right)\right]}{\bar{\gamma}_{12}}\right). \end{aligned} \tag{61}$$

Remark 5. When $\bar{\gamma}_{S1} \longrightarrow \infty$ and $\bar{\gamma}_{12} \longrightarrow \infty$, the $P_2^{\text{out},FD}$ can be approximated as

$$P_2^{\text{out},FD,\infty} = 1 - \frac{Q^{FD}}{2}\sum_{i=1}^{K}\omega_i H_3(y_i). \tag{62}$$

where

$$\begin{aligned} H_3(y) = {} & A'_{k,t}C_{k_1}\exp\left(-\frac{y}{\bar{\gamma}_{1E}}\right)\left[\frac{k_1!}{\mu^{k_1+1}} - \exp(-\mu y)\sum_{t_1=0}^{k_1}\frac{k_1!}{t_1!}\frac{y^{t_1}}{\mu^{k_1-t_1+1}}\right] \\ & \times\left(\frac{\zeta\left[\bar{\gamma}_2^{FD} + y\left(1+\bar{\gamma}_2^{FD}\right)\right]}{\alpha_2 - \left[\bar{\gamma}_2^{FD} + y\left(1+\bar{\gamma}_2^{FD}\right)\right]\alpha_1}\right)^t \\ & \times\exp\left(\frac{-\Delta'_{S1}\zeta\left[\bar{\gamma}_2^{FD} + y\left(1+\bar{\gamma}_2^{FD}\right)\right]}{\alpha_2 - \left[\bar{\gamma}_2^{FD} + y\left(1+\bar{\gamma}_2^{FD}\right)\right]\alpha_1}\right), \\ A'_{k,t} = {} & \alpha_{S1}\sum_{k=0}^{m_{S1}-1}\sum_{t=0}^{k}\frac{(1-m_{S1})_k(-\delta_{S1})^k}{k!t!\left(\Delta'_{S1}\right)^{k-t+1}}, \end{aligned} \tag{63}$$

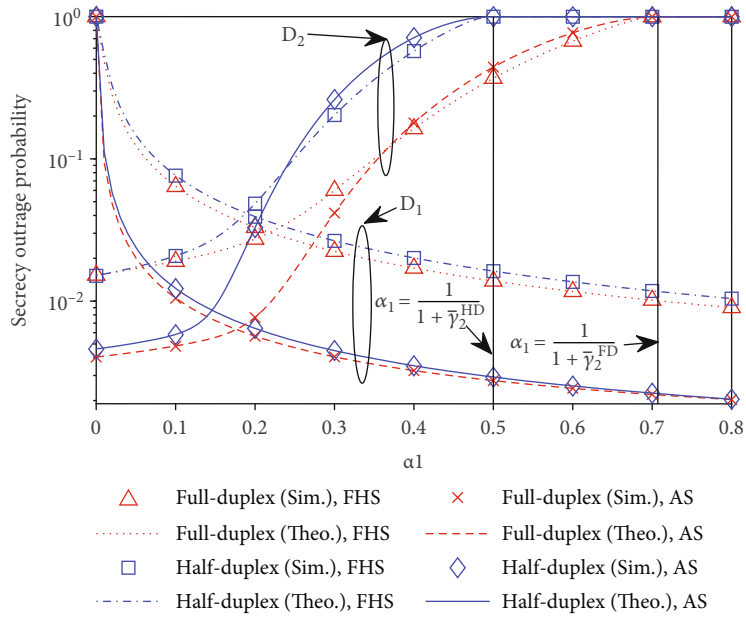

Figure 7: SOP versus α_1.

and $\Delta'_{S1} = \beta_{S1} - \delta_{S1}$. It can be shown that the SOP of D_2 saturates in the high SNR region, which is caused by the residual self-interference.

Remark 6. Note that when $\alpha_1 \geq 1/(1+\bar{\gamma}_2^{FD})$, we can have $P_2^{\mathrm{out},FD} = 1$. This means that D_2 will be always in secrecy outage when the power allocation coefficient for D_1 is not smaller than $1/(1+\bar{\gamma}_2^{FD})$. Since $\bar{\gamma}_2^{HD} > \bar{\gamma}_2^{FD}$, we have $1/(1+\bar{\gamma}_2^{FD}) > 1/(1+\bar{\gamma}_2^{HD})$. Thus, based on the analysis in Remark 3, the threshold for the power allocation coefficient for D_1 under the half-duplex mode is larger than that under full-duplex mode. This indicates that more power can be allocated to D_1 under the full-duplex mode than that under the half-duplex mode, provided that the SOP of D_2 is not 1.

6. Numerical Results

In this section, we verify our theoretical results via conducting simulations. The system parameters and channel fading parameters are presented in Tables 1 and 2, respectively, where FHS denotes heavy shadowing and AS denotes average shadowing [16, 18, 37].

Besides, we assume $\bar{\gamma}_{S1} = \bar{\gamma}_{12} = \bar{\gamma} = 30$ dB, $\bar{\gamma}_{SE} = \bar{\gamma}_{1E} = \bar{\gamma}_E = -5$ dB, $R_1 = R_2 = 0.5$ bits/s/Hz, $\zeta = -30$ dB, and $K = 20$ [18, 32, 49].

Figure 2 compares the SOPs with FHS and AS for the near user D_1 under different values of $\bar{\gamma}$. The theoretical results are shown to match well with the simulation results, which verifies the correctness of the theoretical results. As expected, the secrecy outage performance with AS is better than that with FHS. It is seen that compared to the half-duplex mode, the secrecy outage performance under the full-duplex mode is better when $\bar{\gamma}$ is small. When $\bar{\gamma}$ is large, it is seen that the secrecy outage performance under the full-duplex mode saturates and underperforms that under the half-duplex mode. This is consistent with our analysis in Remarks 1 and 4 that the SOP of D_1 under the half-duplex mode does not saturates in the high SNR region, while it saturates under the full-duplex mode. This indicates that the near user prefers the full-duplex mode when the SNR is low and prefers the half-duplex mode when the SNR is high.

Figure 3 compares the SOPs with FHS and AS for the far user D_2 under different values of $\bar{\gamma}$. It is seen that the secrecy outage performance with AS is better than that with FHS, which is expected. When $\bar{\gamma}$ is small, it is seen that the SOP under the full-duplex mode is lower than that under the half-duplex mode. It is also seen that when $\bar{\gamma}$ is large, the SOPs under the full-duplex mode and the half-duplex mode both saturate, which is consistent with the analysis in Remarks 2 and 5. Besides, it is seen that compared to the half-duplex mode, the SOP under the full-duplex mode is higher with FHS and is lower with AS. This indicates that for the far user, the half-duplex mode is preferred only when the SNR is high and the channel fading is severe.

Figures 4 and 5 plot the SOPs of D_1 and D_2 against ζ, respectively. It is seen that the SOP under the full-duplex mode increases as ζ increases, which is expected since higher interference under the full-duplex mode exists with a larger ζ. It is also seen that compared to the half-duplex mode, the SOP under the full-duplex mode is lower when ζ is small and is higher when ζ is large. This indicates that the full-duplex mode is preferred by both the near user and the far user only when ζ is small enough.

Figure 6 plots the SOP versus different values of $\bar{\gamma}_E$. It is seen that as $\bar{\gamma}_E$ increases, the SOP increases. This is because the achievable rate at E is higher with a larger value of $\bar{\gamma}_E$. It is also seen that the impact of $\bar{\gamma}_E$ on the SOP of D_2 is severer

than that on the SOP of D_1. This is because E can overhear the message of D_2 broadcast not only by the satellite source but also by the near user D_1. Besides, it is seen that for D_1, the SOP under the full-duplex mode is lower than that under the half-duplex mode when $\bar{\gamma}_E$ is small and is higher than that under the half-duplex mode when $\bar{\gamma}_E$ is large. It is also seen that for D_2, the SOP under the full-duplex mode is always lower than that under the half-duplex mode. This indicates that $\bar{\gamma}_E$ has no impact on the secrecy outage performance comparison between the half-duplex mode and the full-duplex mode for the far user.

Figure 7 plots the SOP versus different values of α_1. It is seen that as α_1 increases, the SOP of D_1 decreases, while the SOP of D_2 increases. This indicates that allocating more power to the users can lead to lower SOP. When α_1 is larger than a certain threshold, it is seen that the SOP of D_2 is constant at 1, which is consistent with the analysis in Remarks 3 and 6. It is also seen that such threshold under the full-duplex mode is larger than that under the half-duplex mode, which is also consistent with the analysis in Remark 6. And it is seen that under the given settings, the full-duplex mode always outperforms the half-duplex mode whatever the value of α_1 is. This indicates that α_1 has no impact on the secrecy outage performance comparison between the half-duplex mode and the full-duplex mode for both the near user and the far user. Besides, it is shown that the secrecy outage performance of D_2 with FHS in the high α_1 region is better than that with AS. This is explained as follows. When α_1 is large enough, the SNR for decoding x_2 at D_2 is constrained by the SNR for decoding x_2 at D_1. When the channel condition becomes worse, although the desired signal for decoding x_2 at D_1 is weakened, the interference signal is also weakened, which slows down the decrease in the SNR, whereas due to the use of PIC, the interference signal for decoding x_2 at E is assumed to be perfectly cancelled. Therefore, the channel condition has severer impact on the SNR at E than that at D_2 when α_1 is large enough, which results in better secrecy outage performance of D_2 with FHS compared to that with AS in the high α_1 region.

7. Conclusion

This paper investigates the SOP of a downlink CNOMA-assisted hybrid satellite-terrestrial network, where there is no direct link between the satellite source and the far terrestrial user, and the near terrestrial user acts as a relay to forward the information to the far terrestrial user under the half-duplex mode or the full-duplex mode. The closed-form exact expressions for the SOP of the near user and the closed-form approximate expressions for the SOP of the far user are derived. It is shown that the theoretical results match well with the simulation results. It is also shown that compared to the half-duplex mode, the full-duplex mode is superior when the received SNR at the near user is low or the residual self-interference is low.

Data Availability

No data were used to support this study.

Conflicts of Interest

The authors declare that they have no conflicts of interest regarding the publication of this article.

Acknowledgments

This work was supported by the Jiangsu Provincial Key Research and Development Program under Grant BE2021013-2.

References

[1] S. Kota, G. Giambene, and S. Kim, "Satellite component of NGN: integrated and hybrid networks," *International Journal of Satellite Communications and Networking*, vol. 29, no. 3, pp. 191–208, 2011.

[2] S. Sreng, B. Escrig, and M.-L. Boucheret, "Exact symbol error probability of hybrid/integrated satellite-terrestrial cooperative network," *IEEE Transactions on Wireless Communications*, vol. 12, no. 3, pp. 1310–1319, 2013.

[3] K. Y. Jo, *Satellite Communications Network Design and Analysis*, Artech house, 2011.

[4] Z. Ding, X. Lei, G. K. Karagiannidis, R. Schober, J. Yuan, and V. K. Bhargava, "A survey on non-orthogonal multiple access for 5G networks: research challenges and future trends," *IEEE Journal on Selected Areas in Communications*, vol. 35, no. 10, pp. 2181–2195, 2017.

[5] B. Evans, M. Werner, E. Lutz et al., "Integration of satellite and terrestrial systems in future multimedia communications," *IEEE Wireless Communications*, vol. 12, no. 5, pp. 72–80, 2005.

[6] V. K. Sakarellos, C. Kourogiorgas, and A. D. Panagopoulos, "Cooperative hybrid land mobile satellite–terrestrial broadcasting systems: outage probability evaluation and accurate simulation," *Wireless Personal Communications*, vol. 79, no. 2, pp. 1471–1481, 2014.

[7] Y. Liu, Z. Qin, M. Elkashlan, Z. Ding, A. Nallanathan, and L. Hanzo, "Nonorthogonal multiple access for 5G and beyond," *Proceedings of the IEEE*, vol. 105, no. 12, pp. 2347–2381, 2017.

[8] R. Liu, K. Guo, K. An, S. Zhu, and H. Shuai, "Joint decoding order and power allocation design for a NOMA-based overlay cognitive integrated satellite-terrestrial relay network," *Wireless Communications and Mobile Computing*, vol. 2022, Article ID 2638461, 2022.

[9] D. Xu and H. Zhu, "Sum-rate maximization of wireless powered primary users for cooperative CRNs: NOMA or TDMA at cognitive users?," *IEEE Transactions on Communications*, vol. 69, no. 7, pp. 4862–4876, 2021.

[10] Z. Ding, M. Peng, and H. V. Poor, "Cooperative non-orthogonal multiple access in 5G systems," *IEEE Communications Letters*, vol. 19, no. 8, pp. 1462–1465, 2015.

[11] R. Lei, D. Xu, and I. Ahmad, "Secrecy outage performance analysis of cooperative NOMA networks with SWIPT," *IEEE Wireless Communications Letters*, vol. 10, no. 7, pp. 1474–1478, 2021.

[12] R. Lei and D. Xu, "On the outage performance of JT-CoMP-CNOMA networks with SWIPT," *IEEE Communications Letters*, vol. 25, no. 2, pp. 432–436, 2021.

[13] B. Li, D. Xu, B. Chen, and I. Ahmad, "Outage performance of CoMP-CNOMA networks with duplex mode selection," *Physical Communication*, vol. 52, article 101701, 2022.

[14] X. Yan, H. Xiao, C.-X. Wang, and K. An, "Outage performance of NOMA-based hybrid satellite-terrestrial relay networks," *IEEE Wireless Communications Letters*, vol. 7, no. 4, pp. 538–541, 2018.

[15] N.-L. Nguyen, H.-N. Nguyen, A.-T. Le, D.-T. Do, and M. Voznak, "On performance analysis of NOMA-aided hybrid satellite terrestrial relay with application in small-cell network," *IEEE Access*, vol. 8, pp. 188526–188537, 2020.

[16] K. Guo, K. An, F. Zhou, T. A. Tsiftsis, G. Zheng, and S. Chatzinotas, "On the secrecy performance of NOMA-based integrated satellite multiple-terrestrial relay networks with hardware impairments," *IEEE Transactions on Vehicular Technology*, vol. 70, no. 4, pp. 3661–3676, 2021.

[17] K. Guo, K. An, B. Zhang, Y. Huang, and D. Guo, "Physical layer security for hybrid satellite terrestrial relay networks with joint relay selection and user scheduling," *IEEE Access*, vol. 6, pp. 55815–55827, 2018.

[18] V. Bankey and P. K. Upadhyay, "Physical layer security of multiuser multirelay hybrid satellite-terrestrial relay networks," *IEEE Transactions on Vehicular Technology*, vol. 68, no. 3, pp. 2488–2501, 2019.

[19] P. Chini, G. Giambene, and S. Kota, "A survey on mobile satellite systems," *International Journal of Satellite Communications and Networking*, vol. 28, no. 1, pp. 29–57, 2010.

[20] K. An, M. Lin, and T. Liang, "On the performance of multiuser hybrid satellite-terrestrial relay networks with opportunistic scheduling," *IEEE Communications Letters*, vol. 19, no. 10, pp. 1722–1725, 2015.

[21] K. Guo, K. An, B. Zhang et al., "On the performance of the uplink satellite multiterrestrial relay networks with hardware impairments and interference," *IEEE Systems Journal*, vol. 13, no. 3, pp. 2297–2308, 2019.

[22] K. An, T. Liang, G. Zheng, X. Yan, Y. Li, and S. Chatzinotas, "Performance limits of cognitive-uplink FSS and terrestrial FS for Ka-band," *IEEE Transactions on Aerospace and Electronic Systems*, vol. 55, no. 5, pp. 2604–2611, 2019.

[23] Z. Lin, M. Lin, T. de Cola, J.-B. Wang, W.-P. Zhu, and J. Cheng, "Supporting IoT with rate-splitting multiple access in satellite and aerial-integrated networks," *IEEE Internet of Things Journal*, vol. 8, no. 14, pp. 11123–11134, 2021.

[24] Z. Lin, M. Lin, B. Champagne, W.-P. Zhu, and N. Al-Dhahir, "Secure and energy efficient transmission for RSMA-based cognitive satellite-terrestrial networks," *IEEE Wireless Communications Letters*, vol. 10, no. 2, pp. 251–255, 2021.

[25] Z. Lin, M. Lin, J.-B. Wang, T. de Cola, and J. Wang, "Joint beamforming and power allocation for satellite-terrestrial integrated networks with non-orthogonal multiple access," *IEEE Journal of Selected Topics in Signal Processing*, vol. 13, no. 3, pp. 657–670, 2019.

[26] H. Shuai, K. Guo, K. An, and S. Zhu, "NOMA-based integrated satellite terrestrial networks with relay selection and imperfect SIC," *IEEE Access*, vol. 9, pp. 111346–111357, 2021.

[27] Z. Lin, H. Niu, K. An et al., "Refracting RIS aided hybrid satellite-terrestrial relay networks: joint beamforming design and optimization," *IEEE Transactions on Aerospace and Electronic Systems*, p. 1, 2022, to be published.

[28] K. Guo and K. An, "On the performance of RIS-assisted integrated satellite-UAV-terrestrial networks with hardware impairments and interference," *IEEE Wireless Communications Letters*, vol. 11, no. 1, pp. 131–135, 2022.

[29] B. M. ElHalawany, R. Ruby, T. Riihonen, and K. Wu, "Performance of cooperative NOMA systems under passive eavesdropping," in *2018 IEEE Global Communications Conference (GLOBECOM)*, pp. 1–6, Abu Dhabi, United Arab Emirates, 2018.

[30] R. Ruby, Q.-V. Pham, K. Wu, A. A. Heidari, H. Chen, and B. M. ElHalawany, "Enhancing secrecy performance of cooperative NOMA-based IoT networks via multiantenna-aided artificial noise," *IEEE Internet of Things Journal*, vol. 9, no. 7, pp. 5108–5127, 2022.

[31] H. B. Nesrine Zaghdoud, A. B. Mnaouer, and F. Touati, "Secrecy performance analysis of half/full duplex AF/DF relaying in NOMA systems over κ–μ fading channels," *Telecommunication Systems*, vol. 79, no. 2, pp. 213–231, 2022.

[32] H.-N. Nguyen, N.-L. Nguyen, N.-T. Nguyen et al., "Reliable and secure transmission in mul-tiple antennas hybrid satellite-terrestrial cognitive networks relying on NOMA," *IEEE Access*, vol. 8, pp. 215044–215056, 2020.

[33] K. An, M. Lin, J. Ouyang, and W.-P. Zhu, "Secure transmission in cognitive satellite terrestrial networks," *IEEE Journal on Selected Areas in Communications*, vol. 34, no. 11, pp. 3025–3037, 2016.

[34] K. Guo, C. Dong, and K. An, "NOMA-based cognitive satellite terrestrial relay network: secrecy performance under channel estimation errors and hardware impairments," *IEEE Internet of Things Journal*, 2022, to be published.

[35] K. Guo, M. Lin, B. Zhang et al., "Performance analysis of hybrid satellite-terrestrial cooperative networks with relay selection," *IEEE Transactions on Vehicular Technology*, vol. 69, no. 8, pp. 9053–9067, 2020.

[36] K. An, M. Lin, J. Ouyang, Y. Huang, and G. Zheng, "Symbol error analysis of hybrid satellite–terrestrial cooperative networks with cochannel interference," *IEEE Communications Letters*, vol. 18, no. 11, pp. 1947–1950, 2014.

[37] A. Abdi, W. C. Lau, M.-S. Alouini, and M. Kaveh, "A new simple model for land mobile satellite channels: first- and second-order statistics," *IEEE Transactions on Wireless Communications*, vol. 2, no. 3, pp. 519–528, 2003.

[38] P. Series, *Prediction procedure for the evaluation of interference between stations on the surface of the Earth at frequencies above about 0.1 GHz; ITU-R P.452-15*, ITU: Geneva, Switzerland, 2013.

[39] K. Guo, M. Lin, B. Zhang, W.-P. Zhu, J.-B. Wang, and T. A. Tsiftsis, "On the performance of LMS communication with hardware impairments and interference," *IEEE Transactions on Communications*, vol. 67, no. 2, pp. 1490–1505, 2018.

[40] D. Zwillinger and A. Jeffrey, *Table of Integrals, Series, and Products*, Elsevier, 2007.

[41] W. Cao, Y. Zou, Z. Yang, and J. Zhu, "Relay selection for improving physical-layer security in hybrid satellite-terrestrial relay networks," *IEEE Access*, vol. 6, pp. 65275–65285, 2018.

[42] X. Li, J. Li, Y. Liu, Z. Ding, and A. Nallanathan, "Residual transceiver hardware impairments on cooperative NOMA networks," *IEEE Transactions on Wireless Communications*, vol. 19, no. 1, pp. 680–695, 2020.

[43] M. S. Ali, H. Tabassum, and E. Hossain, "Dynamic user clustering and power allocation for uplink and downlink non-orthogonal multiple access (NOMA) systems," *IEEE Access*, vol. 4, pp. 6325–6343, 2016.

[44] H. Lei, J. Zhang, K.-H. Park et al., "Secrecy outage of max–min TAS scheme in MIMO-NOMA systems," *IEEE Transactions on Vehicular Technology*, vol. 67, no. 8, pp. 6981–6990, 2018.

[45] Y. Liu, Z. Qin, M. Elkashlan, Y. Gao, and L. Hanzo, "Enhancing the physical layer security of non-orthogonal multiple access in large-scale networks," *IEEE Transactions on Wireless Communications*, vol. 16, no. 3, pp. 1656–1672, 2017.

[46] M. Duarte, C. Dick, and A. Sabharwal, "Experiment-driven characterization of full-duplex wireless systems," *IEEE Transactions on Wireless Communications*, vol. 11, no. 12, pp. 4296–4307, 2012.

[47] H. Q. Ngo, H. A. Suraweera, M. Matthaiou, and E. G. Larsson, "Multipair full-duplex relaying with massive arrays and linear processing," *IEEE Journal on Selected Areas in Communications*, vol. 32, no. 9, pp. 1721–1737, 2014.

[48] D. Li, Y. Cao, Z. Yang et al., "Secrecy analysis in NOMA full-duplex relaying networks with artificial jamming," *IEEE Transactions on Vehicular Technology*, vol. 70, no. 9, pp. 8781–8794, 2021.

[49] Y. Alsaba, C. Y. Leow, and S. K. A. Rahim, "Full-duplex cooperative non-orthogonal multiple access with beamforming and energy harvesting," *IEEE Access*, vol. 6, pp. 19726–19738, 2018.

[50] K. Guo, K. An, Y. Huang, and B. Zhang, "Physical layer security of multiuser satellite communication systems with channel estimation error and multiple eavesdroppers," *IEEE Access*, vol. 7, pp. 96253–96262, 2019.

[51] C. Yu, H.-L. Ko, X. Peng, W. Xie, and P. Zhu, "Jammer-aided secure communications for cooperative NOMA systems," *IEEE Communications Letters*, vol. 23, no. 11, pp. 1935–1939, 2019.

[52] M. Abramowitz, I. A. Stegun, and R. H. Romer, *Handbook of Mathematical Functions with Formulas, Graphs, and Mathematical Tables*, New York, NY, USA: Dover, 9th edition, 1972.